

Statistics of Impedance and Scattering Matrices of Chaotic Microwave Cavities with Multiple Ports

Xing Zheng, Thomas M. Antonsen Jr.,* and Edward Ott*

Department of Physics

and Institute for Research in Electronics and Applied Physics,

University of Maryland, College Park, MD, 20742

(Dated: June 29, 2018)

The statistical model proposed in an accompanying paper is generalized to treat multiport scattering problems. Attention is first focused on two-port lossless systems and the model is shown to be consistent with Random Matrix Theory. The predictions are then tested by direct numerical simulation for a specific two-port cavity. Formulae are derived for the average transmission and reflection coefficients in terms of the port radiation impedance. The cases of cavities with multiple ports, and with a single port and distributed losses are compared.

Keywords: wave chaos, impedance, scattering matrix

I. INTRODUCTION

In an accompanying paper [1], a general statistical model is proposed to describe scattering of high frequency electromagnetic waves from irregular cavities (Here by high frequency we mean that the wavelength is substantially less than an appropriate characteristic length of the cavity.). This problem arises when one considers the coupling of electromagnetic energy into and out of complicated enclosures. The statistical approach is warranted when the exact details of the configuration are unknown or are too complicated to simulate accurately. The model proposed in Ref. [1] gives a method for calculating the statistical distributions of important quantities that depend only on a small number of system-specific parameters. These system-specific parameters are the average spacing between resonant frequencies of the enclosure, the average quality factor, and the properties of the coupling ports. It was shown [1] that the key property needed to characterize the coupling port is its radiation impedance, that is, the impedance that would be seen at the port if the other boundaries of the enclosure were perfectly absorbing or were removed to infinity. This impedance can be used to “normalize” the fluctuating impedance at the port of the actual enclosure. With this normalization the fluctuating impedance has a universal (i.e., system-specific independent) distribution.

The treatment in Ref. [1] focused on the case of a single port. The purpose of the present paper is to generalize these results to the case of multiple ports. A multiple port description is necessary if one is to describe the transmission of energy entering the enclosure to some other point in the enclosure. We will show that the multiple port case can be treated using the same approach as the single port case. The main difference being that the multiple port description involves the introduction of matrices describing the coupling to the system.

Scattering can be described by either the impedance matrix, which relates voltages and currents at the ports, or by the scattering matrix, which relates the amplitudes of incoming and outgoing waves. In our model we focus initially on the impedance matrix because its properties can be related directly to the radiation impedances of the ports. Then based on our understanding of the impedance matrix, conclusions about the scattering matrix are drawn.

The statistical treatment of wave scattering in complicated systems has been developed extensively in the physics community in connection with nuclear scattering [2] and scattering in mesoscopic systems such as quantum dots [3] and disordered conductors [4]. Many of the concepts developed in consideration of these problems have also been applied to electromagnetic scattering in microwave cavities [5, 6, 7, 8, 9]. The underlying approach is a description of the system based on random matrix theory (RMT)[10, 11, 12]. Here, the specific systems under consideration are replaced or modelled by random matrices. These are matrices whose elements are independent Gaussian random numbers drawn from specific ensemble distributions. Two different ensembles that are considered are relevant to our problem. The Gaussian Orthogonal Ensemble (GOE) gives rise to a real symmetric matrix, where the variance of the diagonal elements is twice that of the off-diagonal elements. This applies to wave systems with time reversal symmetry (TRS), as would apply in media with real symmetric permittivity and permeability tensors. The Gaussian Unitary Ensemble (GUE) gives rise to complex, self-adjoint matrices, where the off-diagonal elements have independent real and imaginary parts. This applies to wave systems that have time reversal symmetry broken (TRSB). For electromagnetic wave systems, this case is realized when a nonreciprocal medium such as magnetized ferrite or a magnetized cold plasma is present in the system.

Random matrix theory, in spite of its high level of abstraction, has been remarkably successful in predicting the universal statistical properties of wave systems. This includes the description of the distribution of resonances

*Also at Department of Electrical and Computer Engineering.

in closed systems as well as the properties of scattering from open systems. One issue, that we address here is how to simultaneously account for the universal properties as predicted by RMT and the system-specific properties that depend on details of the coupling. In our approach this connection is made through the radiation impedance of the ports [8] (This connection has also been made by Warne et al. [13]). An alternative approach [14] in the physics community, known as “the Poisson Kernel”, is based directly on the scattering matrix. This approach describes the distribution of fluctuations in the scattering matrix elements in terms of their average values. Recently, Kuhl et. al.[15] applied the Poisson Kernel approach to analyse the statistics of measured values of the reflection coefficient for a microwave cavity. The measured results were found to be in agreement with predictions based on the Poisson kernel.

The organization of this paper is as follows. Section II generalizes the description of the quasi-two dimensional cavity introduced in Ref. [1] to describe the presence of multiple ports. Our treatment will be sufficiently general so as to treat the case of both isolated ports and non-isolated ports. We then discuss the changes that must be made when non-reciprocal elements such as a magnetized ferrite are present. In Sec. III we examine the statistical properties of the proposed impedance matrix, focusing on the two-port case. We also compare the model predictions with the results of computational electromagnetic calculations using HFSS. In Section IV we consider properties of the scattering matrix when the port coupling is imperfect. We find that the average value of the reflection coefficient is a function of the radiation reflection coefficient. Also, we consider the case of multiple ports and verify the equivalence of distributed and diffractive losses in the case of large number of ports. Section V contains a summary of our results. Except for Section IV(B) all our considerations will be in the context of lossless cavities.

II. GENERALIZATION OF THE MODEL

A. The Impedance in the TRS Case

Following Ref.[1] we consider a quasi-two dimensional cavity in which only the lowest order transverse magnetic modes are excited. The fields in the cavity are determined by the spatially dependent phasor amplitude of the voltage $\hat{V}_T(x, y)$. The voltage is excited by currents \hat{I}_i drives at the various coupling ports,

$$(\nabla_{\perp}^2 + k^2)\hat{V}_T = -jkh\eta_0 \sum_{i=1}^M u_i \hat{I}_i. \quad (1)$$

Here $k = \omega/c$, $\eta_0 = \sqrt{\mu_0/\epsilon_0}$, h is the height of the cavity and an exponential time dependence $\exp(j\omega t)$ has been assumed for all time dependent quantities. Each of the M ports is characterized by a profile function u_i

centered at different locations and $\int dx dy u_i = 1$. The phasor voltage at each port can be calculated as before, $\hat{V}_i = \int dx dy u_i \hat{V}_T \equiv \langle u_i \hat{V}_T \rangle$ and is linearly related to the phasor currents \hat{I}_j through the impedance matrix, $\hat{V}_i = \sum_j Z_{ij} \hat{I}_j$.

To obtain an expression for the matrix Z , we expand \hat{V}_T as before [1] in the basis ϕ_n , the eigenfunctions of the closed cavity. The result is

$$Z = -jkh\eta_0 \sum_n \frac{\Phi_n \Phi_n^T}{k^2 - k_n^2}, \quad (2)$$

where the vector Φ_n is $[\langle u_1 \phi_n \rangle, \langle u_2 \phi_n \rangle, \dots, \langle u_M \phi_n \rangle]^T$. Using the random eigenfunction hypothesis, we write ϕ_n as a superposition of random plane waves. Thus the elements of the M -dimensional vector Φ_n will be Gaussian random variables with zero mean. Elements of Φ_n with different values of n corresponding to different eigenfunctions will be independent. However, for a given eigenfunction the elements of Φ_n may be correlated. This will be true, particularly, if two ports are close together, because the random superposition of plane waves leads to an autocorrelation function $J_0(k\delta r)$ at two positions separated by δr [16]. To treat correlations we write

$$\Phi_n = L(k_n)w_n, \quad (3)$$

where L is a non-random, as yet unspecified, $M \times M$ matrix that depends on the specific coupling geometry at the ports and may depend smoothly on k_n , and w_n is an M -dimensional Gaussian random vector with zero mean and covariance matrix equal to the $M \times M$ identity matrix. That is we require that the components of the random vector w_n are statistically independent of each other, each with unit variance. Correlations between ports are described by the off-diagonal components of L . The idea behind (3) is that the excitation of the ports by an eigenmode will depend on the port geometry and on the structure of the eigenmode in the vicinity of the ports. The dependence on the specific port geometry is not sensitive to small changes in the frequency or cavity configuration and is embodied in the matrix quantity $L(k)$. The structure of the eigenmode in the vicinity of the ports, however, is very sensitive to the frequency and cavity configuration, and this motivates the statistical treatment via the random plane wave hypothesis. From the random plane wave hypothesis, the excitation of the port from a given plane wave component is random, and, since many such waves are superposed, by the central limit theorem, the port excitation is a Gaussian random variable, as reflected by the vector w_n . In Paper I, we have derived a result equivalent to (3) for the case of a one-port with a specific model of the excitation at the port (namely, a vertical source current density $Iu(x, y)\hat{z}$ between the plates). Our derivation here will be more general in that it does not depend on a specific excitation or on the two-dimensional cavity configuration used in Paper I. Thus this derivation applies, for example, to

three dimensional cavities, and arbitrary port geometries. From (2) and (3) we have for the Z matrix

$$Z = -jkh\eta_0 \sum_n \frac{L(k_n)w_n w_n^T L^T(k_n)}{k^2 - k_n^2}. \quad (4)$$

We now take the continuum limit of (4) and average over w_n ,

$$\langle Z \rangle = -j \int_0^\infty kh\eta_0 L(k') \frac{\langle w_n w_n^T \rangle}{k^2 - (k')^2} L^T(k') \frac{dk'}{\Delta}, \quad (5)$$

where Δ is the averaged spacing in k_n^2 values. We note that the continuum limit is approached as the size of the cavity is made larger and larger, thus making the resonance spacing ($k_{n+1}^2 - k_n^2$) approach zero. Thus, the continuum limit corresponds to moving the lateral walls of the cavity to infinity. Using our previous one-port argument as a guide, we anticipate that, if the pole in Eq. (5) at $k'^2 = k^2$ is interpreted in the causal sense (corresponding to outgoing waves in the case with the walls removed to infinity), then $\langle Z \rangle$ in (5) is the radiation impedance matrix,

$$\langle Z \rangle = Z_R(k) = \hat{R}_R(k) + j\hat{X}_R(k), \quad (6)$$

where $\hat{V} = Z_R(k)\hat{I}$ with \hat{V} the M -dimensional vector of port voltages corresponding to the M -dimensional vector of port currents \hat{I} , in the case where the lateral walls have been removed to infinity. With the above interpretation of the pole, the real part of Eq. (5) yields

$$\hat{R}_R(k) = \pi kh\eta_0 L(k) L^T(k) / \Delta. \quad (7)$$

Thus, Eq. (2) becomes

$$Z = -\frac{j}{\pi} \sum_n \Delta \frac{\hat{R}_R^{1/2}(k_n) w_n w_n^T \hat{R}_R^{1/2}(k_n)}{k^2 - k_n^2}, \quad (8)$$

where $\langle w_n w_n^T \rangle = 1_M$. (Note that the formula for Δ is different in two and three dimensions.) In the case of transmission line inputs that are far apart, e.g., of the order of the cavity size, then the off-diagonal elements of Z_R are small and can be neglected. On the other hand, this will not be the case if some of the transmission line inputs are separated from each other by a short distance of the order of a wavelength. Similarly, if there is a waveguide input to the cavity where the waveguide has multiple propagating modes, then there will be components of \hat{V} and \hat{I} for each of these modes, and the corresponding off-diagonal elements of Z_R for coupling between these modes will not be small.

For the remainder of the paper, we will assume identical transmission line inputs that are far enough apart that we may neglect the off-diagonal elements of Z_R . As before, we will take the eigenvalues k_n^2 to have a distribution generated by RMT. Because the elements of Z depend on the eigenvalues k_n^2 , there will be correlations among the elements. In the lossless case the elements of

the Z matrix are imaginary, $Z = jX$, where X is a real symmetric matrix. Consequently X has real eigenvalues. We will show in Sec. III that the distribution for individual eigenvalues of X is Lorentzian with mean and width determined by the corresponding radiation impedance.

B. Effects of Time-Reversal Symmetry Breaking (TRSB)

In the time-reversal symmetric system, the eigenfunctions of the cavity are real and correspond to superpositions of plane waves with equal amplitude waves propagating in opposite directions as in Eq. (13) of paper [1], which is recalled as follows

$$\phi_n = \lim_{N \rightarrow \infty} \sqrt{\frac{2}{AN}} \text{Re} \left\{ \sum_{i=1}^N \alpha_i \exp(jk_n \vec{e}_i \cdot \vec{x} + j\theta_i) \right\}, \quad (9)$$

where α_i , θ_i and \vec{e}_i are random variables. If a non-reciprocal element (such as a magnetized ferrite) is added to the cavity, then time reversal symmetry is broken (TRSB). As a consequence, the eigenfunctions become complex. Eq. (9) is modified by removal of the operation of taking the real part, and the $\langle u\phi_n \rangle$ in Eq. (12) of paper [1] also become complex. In practice, there exists a crossover regime for the transition from situations where time reversal symmetry applies to those it is fully-broken. An interested reader might refer to situations where discussion in Ref. [6] and the references therein. However, in this paper, we will discuss only the case when time-reversal symmetry is fully broken. In this case we find

$$\langle u_\ell \phi_n \rangle = [\Delta \hat{R}_R(k_n)]^{1/2} w_{\ell n} \quad (10)$$

where $w_{\ell n} = (w_{\ell n}^{(r)} + jw_{\ell n}^{(i)})/\sqrt{2}$ and $w_{\ell n}^{(r)}$ and $w_{\ell n}^{(i)}$ are real, independent Gaussian random variables with zero mean and unit variance. The extra factor of $\sqrt{2}$ accounts for the change in the normalization factor in Eq. (9), required when the eigenfunctions become complex. Further, transpose w_n^T , in Eq. (8) is now replaced by the conjugate transpose w_n^\dagger .

A further consequence of TRSB is that the distribution of eigenvalues is changed. The main difference is the behavior of $P(s)$ for small s . In particular, the probability of small spacings in a TRSB system ($P(s) \sim s^2$) is less than that of a TRS system ($P(s) \sim s$).

For the sake of simplicity, we will assume all the transmission lines feeding the cavity ports are identical, and have the same radiation impedance, $Z_R = \hat{R}_R + j\hat{X}_R = (R_R + jX_R)1_M$, where R_R and X_R are real scalars. Analogous to the one port case, we can define a model normalized reactance matrix $\xi_{ij} = X_{ij}/R_R$ for the case $R_R(k_n)$ constant for $n \leq N$ and $R_R(k_n) = 0$ for $n > N$,

$$\xi_{ij} = -\frac{1}{\pi} \sum_{n=1}^N \frac{w_{in} w_{jn}^*}{k^2 - k_n^2}, \quad (11)$$

where $\tilde{k}^2 = k^2/\Delta$, $w_{\ell n} = (w_{\ell n}^{(r)} + jw_{\ell n}^{(i)})/\sqrt{2}$, $w_{\ell n}^{(r)}$ and $w_{\ell n}^{(i)}$ are real, independent Gaussian random variables with zero mean and unit variance, $E(w_{in}^* w_{jn}) = \delta_{ij}$. Note that a unitary transformation, $\xi' = U\xi U^\dagger$, returns (11) with w_{in} and w_{jn} replaced by w'_{in} and w'_{jn} where $w'_n = Uw_n$. Since a unitary transformation does not change the covariance matrix, $E(w_{in} w_{jn}^*) = E(w'_{in} w'_{jn}^*) = \delta_{ij}$, the statistics of ξ and of ξ' are the same; i.e., their statistical properties are invariant to unitary transformations.

III. PROPERTIES OF THE IMPEDANCE MATRIX AND EIGENVALUE CORRELATIONS FOR LOSSLESS CAVITIES

The universal fluctuation properties of the Z matrix can be described by the model matrix ξ_{ij} specified in Eq. (11). In the TRS case the w_{jn} are real Gaussian random variables with zero mean and unit width and the spacings satisfy Eq. (16) in Ref. [1]. In the TRSB case the w_{jn} are complex and the spacings between adjacent k_n^2 satisfy Eq. (17) in Ref. [1].

In the case under consideration of multiple identical ports, ξ_{ij} will have a diagonal mean part $\bar{\xi}\delta_{ij}$ for which all the diagonal values are equal. The eigenfunctions of $\xi_{ij} = \bar{\xi}\delta_{ij} + \tilde{\xi}_{ij}$ and of its fluctuating part $\tilde{\xi}_{ij}$ will thus be the same. Consequently, we focus on the eigenvalues of the fluctuating part.

We initially restrict our considerations to the two-port case. We recall that for the lossless one-port case there is no difference in the statistics of the normalized impedance ξ for the TRS and TRSB cases. In both cases, it is Lorentzian with unit width. In the lossless two-port case, however, essential differences are observed when time reversal is broken. Using (11), we generate 10^6 realizations of the 2 by 2 matrix ξ in both the TRS and TRSB cases, again for $N = 2000$ and $k^2 = 1000$. In this test we generated spectra based on an independent spacings [1]. For each realization we compute the eigenvalues of the ξ matrix. We find that in both the TRS and TRSB cases the eigenvalues of the ξ -matrix are Lorentzian distributed with unit width. That is, histograms of the eigenvalues generated according to the TRS and TRSB prescriptions are identical. However, if we consider the joint probability density function (PDF) of the two eigenvalues for each realization, then differences between the TRS and TRSB cases emerge. We map the two eigenvalues ξ_i , $i = 1$ or 2 , into the range $[\pi/2, \pi/2]$ via the transformation $\theta_i = \arctan(\xi_i)$. Scatter plots of θ_2 and θ_1 for 10^6 random numerical realizations of the ξ matrix are shown in Fig. 1(a) for the TRS case and in Fig. 1(b) for the TRSB case. The white diagonal band in both cases shows that the eigenvalues avoid each other (i.e., they are anti-correlated). This avoidance is greater in the TRSB case than in the TRS case. The correlation,

$$\text{corr}(\theta_1, \theta_2) \equiv \frac{\langle \theta_1 \theta_2 \rangle - \langle \theta_1 \rangle \langle \theta_2 \rangle}{\sqrt{\langle \theta_1^2 \rangle \langle \theta_2^2 \rangle}}, \quad (12)$$

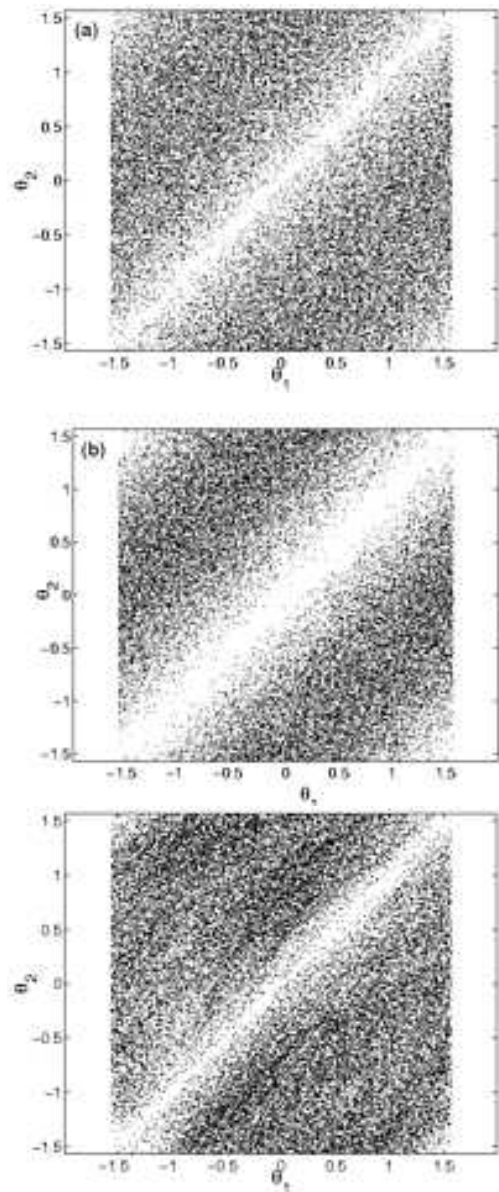


FIG. 1: (a) Scatter plot of θ_1 vs θ_2 , in the TRS case. (b) Scatter plot of θ_1 vs θ_2 in the TRSB case. (c) Scatter plot of θ_1 vs θ_2 from the HFSS simulation, with 100 realizations and sweeping frequency from 6.75GHz to 8.75GHz.

is numerically determined to be -0.216 for the TRS case and -0.304 for the TRSB case.

From the construction of the ξ matrices for the TRS and TRSB cases their statistical properties are invariant under orthogonal and unitary transformations, respectively. Random matrix theory has been used to study these rotation-invariant ensembles and predicts the joint density function of θ_1 and θ_2 [11] to be,

$$P_\beta(\theta_1, \theta_2) \propto |e^{j2\theta_1} - e^{j2\theta_2}|^\beta, \quad (13)$$

where $\beta = 1$ for the TRS case and $\beta = 2$ for the TRSB case. Note that based on Eq. (13), the probability density

function for one of the angles $P(\theta_1) = \int d\theta_2 P(\theta_1, \theta_2)$ is uniform. From the definition $\theta = \arctan \xi$, this is equivalent to the eigenvalues of the ξ matrix having Lorentzian distributions ($P_\xi(\xi_i) = P_\theta(\theta_i) |d\theta_i/d\xi_i| = |d\theta_i/d\xi_i|/2\pi$).

The correlation coefficients calculated from the numerical results in Figs. 1(a) and 1(b) are consistent with the predictions of the random matrix theory from Eq. (13), that is, -0.216 for the TRS case and -0.304 for the TRSB case. This implies that the distribution of spacings and the long range correlations in the eigenvalues of the random matrix, which are ignored in the construction of the k_n^2 in the above computation are not important in describing the statistics of *lossless* impedance matrices. As we have discussed in [1], these correlations could be included using a sequence of k_n^2 generated by the eigenvalues of a random matrix. (We note that [1], lossy cavities yield statistics that are different in the TRS and TRSB cases.)

Now we test these predictions for numerical simulations of the chaotic cavity considered in paper [1]. We use the HFSS software to calculate the cavity impedance matrix and radiation impedance matrix for a 2-port case. We locate the two ports, at the positions $(x, y)=(14\text{cm}, 7\text{cm})$ and $(x, y)=(27\text{cm}, 13.5\text{cm})$. As in [1], we also include the 0.6 cm cylindrical perturbation which is located alternately at 100 random points in the cavity, and we numerically calculate the impedance matrix for 4000 frequencies in the range 6.75GHz to 8.75GHz. We obtain a normalized Z matrix, which is analogous to the ξ matrix defined in Eq. (11) according to

$$\xi_{hfss} = R_R^{-1}(\text{Im}[Z_{cav}] - \mathbf{1}_2 X_R), \quad (14)$$

where $\mathbf{1}_2$ is the 2 by 2 identity matrix, Z_{cav} is the 2 by 2 impedance matrix calculated by HFSS, and X_R and R_R are the radiation reactance and resistance for a single port. For each realization of ξ_{hfss} we calculate its eigenvalues $\xi_i = \tan \theta_i$, $i = 1, 2$, and plot the values on the θ_1 vs. θ_2 plane, as shown in Fig. 1(c). The anti-correlation of the angles is seen in the figure, and $\text{corr}(\theta_1, \theta_2)$ from (12) is -0.205, which is comparable with what we expect for the TRS case, -0.216.

So far we have focused on the eigenvalues of the impedance matrix. The eigenvectors of Z are best described in terms of the orthogonal matrix whose columns are the orthonormal eigenfunctions of Z . Specially, in the TRS case, since ξ is real and symmetric,

$$\xi = O \begin{pmatrix} \tan \theta_1 & 0 \\ 0 & \tan \theta_2 \end{pmatrix} O^T, \quad (15)$$

where O^T is the transpose of O , and O is an orthogonal matrix, which we express in the form

$$O = \begin{pmatrix} \cos \eta & \sin \eta \\ -\sin \eta & \cos \eta \end{pmatrix}. \quad (16)$$

A scatter plot representing the joint pdf of the angle η and one of the eigenvalue angles θ_1 is shown in Fig. 2(a1).

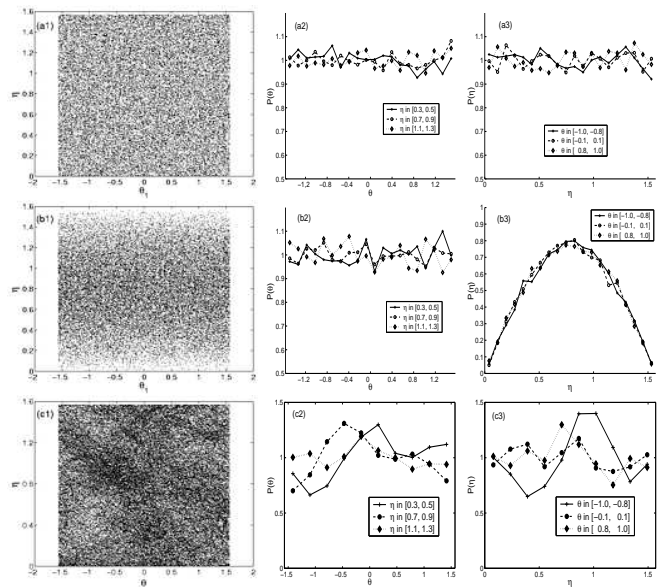


FIG. 2: Scatter plot of η vs θ for (a1) the model impedance in the TRS case, (b1) the model impedance in the TRSB case, and (c1) from the HFSS simulation. Plots (a2) and (a3) [(b2) and (b3), (c2) and (c3)] show conditional probability for θ and for η for the model TRS case [model TRSB case, the HFSS simulation].

In analogy to how we obtain the realizations used in Fig. 2 in [1], this plot is obtained by inserting random choices for the k_n^2 and w_{in} in (11). Notice that we have restricted η in Fig. 2(a1) to the range $0 \leq \eta \leq \pi/2$. This can be justified as follows. The columns of the matrix O in (16) are the eigenvectors of ξ . We can always define an eigenvector such that the diagonal components of O are real and positive. Further, since the eigenvectors are orthogonal, one of them will have a negative ratio for its two components. We pick this one to be the first column and hence this defines which of the two eigenvalues is θ_1 . The scatter plots in Fig. 1 show that the restriction on η maintains the symmetry of θ_1 and θ_2 , vis. $P_\beta(\theta_1, \theta_2) = P_\beta(\theta_2, \theta_1)$. Also in the Fig. 2(a2) (and (a3)), we plot the conditional distribution of θ (and η) for different values of η (and θ). As can be seen, these plots are consistent with η and θ being independent. This is also a feature of the random matrix model [12]. This independence will be exploited later when the S matrix is considered.

For TRSB systems, the ξ matrix is Hermitian $\xi^T = \xi^*$. A unitary matrix of eigenvectors that diagonalizes it can be parameterized as

$$U = \begin{pmatrix} \cos \eta & \sin \eta e^{i\zeta} \\ -\sin \eta e^{-i\zeta} & \cos \eta \end{pmatrix}. \quad (17)$$

Thus, there is an extra parameter ζ characterizing the complex eigenvectors of the ξ matrix. According to random matrix theory, the eigenfunctions and eigenvalues are independently distributed, i.e. η in the U matrix

should be independent of θ_1, θ_2 . This expectation is confirmed in Fig. 2(b) where a scatter plot of θ_1 vs η and conditional distributions of θ and of η are shown.

Again, we test the independence of θ and η with HFSS calculations. Using the ξ_{hfss} matrix obtained from Eq. (14), the angles θ and η can be recovered from the eigenvalues and the eigenvectors of the ξ_{hfss} . With the ensemble generated by sweeping the frequency from 6.75-8.75GHz and considering 100 different locations of our cylindrical perturber, we obtain the joint distribution of θ and η in Fig. 2(c1) as well as their individual distributions in Fig. 2(c2) and (c3). Here we see that the distributions are qualitatively similar to those of the model impedance matrix in the TRS case. However, there are significant departures which need to be investigated. It is likely that these are the result of the same strong multi-path interference which gave rise to the reactance variations in the one port case shown in Paper [1].

IV. AVERAGED REFLECTION COEFFICIENT IN MULTI-PORT CASE

In this section, we use our knowledge of the statistical properties of the Z matrix to deduce properties of the S matrix, particularly for the ensemble average of the reflection coefficient $\langle |S_{11}|^2 \rangle$. For a system with two ports, in the lossless case considered here we note $\langle |S_{12}|^2 \rangle = 1 - \langle |S_{11}|^2 \rangle$

According to the previous section, for the case of non-perfect coupling, model of the cavity impedance matrix can be expressed as $Z = \hat{R}_R^{1/2} \xi \hat{R}_R^{1/2} + j\hat{X}_R$, where Z_R is the 2×2 radiation impedance and ξ is a 2×2 random matrix generated according to Eq. (11). If the incoming frequency is restricted in a narrow range, the radiation impedance Z_R is essentially constant. In this paper we assume that identical ports are connected to identical transmission line, i.e., Z_R and the transmission line characteristic impedance Z_0 are diagonal matrices with equal diagonal elements. Thus, we obtain the expression for the S matrix, $S = (Z + Z_0)^{-1}(Z - Z_0)$,

$$S = [(\gamma_R \xi + j\gamma_X 1_2) + 1_2]^{-1} [(\gamma_R \xi + j\gamma_X 1_2) - 1_2], \quad (18)$$

where $\gamma_R = R_R/Z_0$, $\gamma_X = X_R/Z_0$ are scalars and 1_2 is the 2×2 identity matrix. These two parameters, as we show later, fully specify the coupling effects on the wave transport process. The special case of perfect coupling corresponds to $\gamma_R = 1$ and $\gamma_X = 0$.

A. Lossless Two-port Case

We recall that for TRS systems the reactance matrix X is real and symmetric, and can be diagonalized by an orthogonal matrix O , Eq. (16). If identical ports are connected to identical transmission lines of characteristic impedance Z_0 , then the scattering matrix S is also

diagonalized by O , and we can write

$$S = O \begin{pmatrix} e^{j\phi_1} & 0 \\ 0 & e^{j\phi_2} \end{pmatrix} O^T. \quad (19)$$

The scattering phases ϕ_1 and ϕ_2 are then related to the eigenvalue angles θ_i by formulas analogous to the one-port case, $\tan(\pi/2 - \phi_i/2) = \gamma_R \tan \theta_i + \gamma_X$.

Substituting Eq. (16) for O in (19) and multiplying the matrices, we obtain

$$|S_{11}|^2 = \cos^4 \eta + \sin^4 \eta + 2 \cos^2 \eta \sin^2 \eta \cos(\phi_1 - \phi_2). \quad (20)$$

We can now compute the expected value of the square of $|S_{11}|$ by assuming that η is independent of the angles ϕ_1 and ϕ_2 and is uniformly distributed, which yields $\langle \cos^4 \eta + \sin^4 \eta \rangle = 3/4$, $2 \langle \cos^2 \eta \sin^2 \eta \rangle = 1/4$ and

$$\langle |S_{11}|^2 \rangle = \frac{3}{4} + \frac{1}{4} \langle \cos(\phi_1 - \phi_2) \rangle. \quad (21)$$

Assuming the angles θ_1 and θ_2 are distributed according to Eq. (13) and using the relation between $\phi_{1,2}$ and $\theta_{1,2}$, evaluation of $\langle \cos(\phi_1 - \phi_2) \rangle$ is carried out in Appendix. The result is

$$\langle |S_{11}|^2 \rangle = 1 - \frac{1 - |\rho_R|^4}{8|\rho_R|^2} - \frac{(1 - |\rho_R|^2)^3}{16|\rho_R|^3} \ln \frac{1 - |\rho_R|}{1 + |\rho_R|}, \quad (22)$$

where the ‘‘the free space reflection coefficient’’ ρ_R is defined as the same way in the Paper [1],

$$\rho_R = |\rho_R| e^{j\phi_R} = \frac{\gamma_R + j\gamma_X - 1}{\gamma_R + j\gamma_X + 1}. \quad (23)$$

We first check the asymptotic behavior for the power transmission coefficient $T = 1 - |S_{11}|^2$ implied by the formula (22). In the non-coupled case, $|\rho_R| = 1$, i.e., all the incoming power is reflected, and we obtain from (22) $\langle T \rangle = 0$. On the other hand, in the perfect coupling case, $|\rho_R| = 0$, $\ln[(1 + |\rho_R|)/(1 - |\rho_R|)]$ in the (22) can be expanded as $2(|\rho_R| - |\rho_R|^3/3)$. Therefore, $\langle T \rangle = 1/3$. This is consistent with the result in Ref. [17], $\langle R \rangle = 2\langle T \rangle$. That is, in the perfect coupling case the average of the reflected power is twice that of the transmitted.

Eq. (22) shows that the averaged power reflection and transmission coefficients only depend on the magnitude of ρ_R and not its phase. A plot of $\langle |S_{11}|^2 \rangle$ versus $|\rho_R|$ is shown in Fig. 3(a). Also shown are data points obtained by taking 10^6 realizations of the impedance matrix (11) with eigenvalue statistics generated from TRS spectrum and computing the average of $|S_{11}|^2$ for different combinations of γ_R and γ_X characterizing the radiation impedance. The data confirm that the average of $|S_{11}|^2$ depends only on the magnitude of the free space reflection coefficient and not its phase.

In the TRSB case, the eigenvalues of the X matrix are still real, but the eigenvectors are complex. In this case, Eq. (19) is replaced by

$$S = U \begin{pmatrix} e^{j\phi_1} & 0 \\ 0 & e^{j\phi_2} \end{pmatrix} U^\dagger, \quad (24)$$

where the unitary matrix U is given by Eq. (17). Multiplying the matrices in Eq. (24), we find the same expression for $|S_{11}|^2$, Eq. (20), as in the TRS case. The average of $|S_{11}|^2$ will be different in the TRSB case because of the different statistics for η , θ_1 and θ_2 which characterize the eigenfunctions and eigenvalues of the impedance matrix. In particular, η has a distribution, arising from the SU(2) group [18],

$$P_\eta(\eta) = |\sin(2\eta)|, \quad (25)$$

which yields $\langle \cos^4 \eta + \sin^4 \eta \rangle = 2/3$, $2\langle \cos^2 \eta \sin^2 \eta \rangle = 1/3$, thus,

$$\langle |S_{11}|^2 \rangle = \frac{2}{3} + \frac{1}{3} \langle \cos(\phi_1 - \phi_2) \rangle. \quad (26)$$

Recalling that θ_1 and θ_2 are distributed according to (13) with $\beta = 2$, this results in a different set of integrals (see Appendix). The result is

$$\langle |S_{11}|^2 \rangle = 1 - \frac{(|\rho_R|^2 - 1)(|\rho_R|^2 - 3)}{6}, \quad (27)$$

which depends only on the magnitude of the free space reflection coefficient. A plot of $\langle |S_{11}|^2 \rangle$ from Eq. (27) versus $|\rho_R|$ is also shown in Fig. 3(a), along with data point obtained by taking 10^6 realizations of the TRSB impedance matrix (11) generating from random numbers and computing the average of $|S_{11}|^2$ for different combinations of γ_R and γ_X characterizing the free space impedance. Once again, the data collapse to the curve predicted in Eq. (27).

We now test the relation between $\langle |S_{11}|^2 \rangle$ and $|\rho_R|$ with the impedance matrices we obtained from the HFSS two-port calculations. We can vary the transmission line impedance Z_0 and generate $\langle |S_{11}|^2 \rangle$ and $|\rho_R|$. However, the range of $|\rho_R|$ values accessible doing this is limited because of the large inductive radiation reactance associated with the coupling port. To extend the range of $|\rho_R|$ we add a shunt susceptance $Y = (j\omega C)$ in parallel with each port. This results in a modified cavity impedance matrix $Z'_{cav} = (Z_{cav}^{-1} + j\omega C 1_2)^{-1}$. We then form the scattering matrix

$$S = (Z'_{cav} + Z_0)^{-1}(Z'_{cav} - Z_0). \quad (28)$$

The corresponding free space reflection coefficient is generated by $Z'_R = (Z_R^{-1} + j\omega C)^{-1}$ and $|\rho_R| = |Z'_R + Z_0|^{-1}|Z'_R - Z_0|$. By choosing appropriate combinations of ωC and Z_0 , we can achieve a range of $|\rho_R|$ values between 0 and 1. For each $|\rho_R|$ value, we average $|S_{11}|^2$ over frequencies and realizations and plot the points on Fig. 3(b). These compare favorably with the theoretical result (solid curve) based on the random matrix theory results.

B. M-port Case, $M > 2$

Using the random coupling model (11) and assuming perfect coupling $\gamma_R = 1$, $\gamma_X = 0$ (i.e. $|\rho_R| = 0$), we

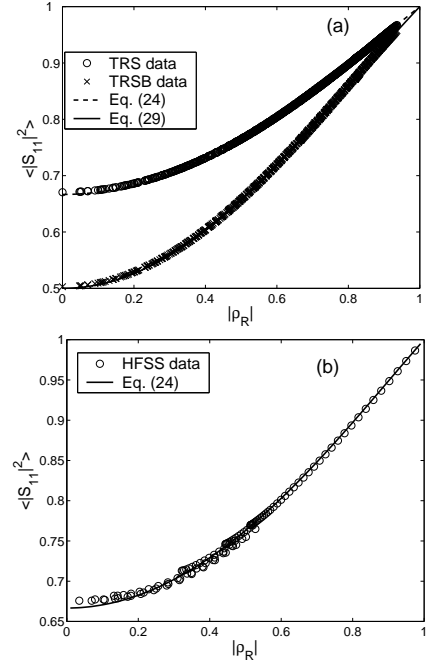


FIG. 3: (a) Numerical simulation for the average reflection coefficient $\langle |S_{11}|^2 \rangle$ vs magnitude of ρ_R defined in Eq. (23) for the TRS and the TRSB system, taking 10^6 realization of the impedance matrix (11) generating from random numbers and computing the average of $|S_{11}|^2$ for different combinations of γ_R and γ_X characterizing the free space impedance. (b) Average reflection coefficient $\langle |S_{11}|^2 \rangle$ vs $|\rho_R|$ using the cavity impedance and radiation impedance from HFSS calculation and varying the values of Z_0 and the capacitive reactance Y

have simulated the S matrix for cases of two to seven, 13 and 57 ports. The results for the average reflection and transmission coefficients were found to satisfy:

$$\text{TRS :} \quad \langle |S_{ij}|^2 \rangle = \begin{cases} \frac{2}{M+1} & i = j, \\ \frac{1}{M+1} & i \neq j, \end{cases} \quad (29)$$

and

$$\text{TRSB :} \quad \langle |S_{ij}|^2 \rangle = \begin{cases} \frac{1}{M} & i = j, \\ \frac{1}{M} & i \neq j, \end{cases} \quad (30)$$

where M is the number of ports connecting the cavity to transmission lines. It seems that, in the TRS case, the input waves “remember” their entry port and have a preference for reflection through it (this is related to the concept of “weak localization” reviewed in [19]). In contrast, for the TRSB case, the waves behave as if they forget through which port they entered the cavity, and thus all the ports have equal probability of being the output for the waves.

It was shown by Brouwer and Beenakker [20] that scattering in multiport lossless systems can be related to that in a single-port, lossy system. It was proposed that the introduction of N' ($N' \gg 1$) fictitious ports into the scattering matrix of a lossless system would give equivalent statistics for the reflection coefficient seen at a single

port as would be obtained for a single port model with a uniform internal loss. Considering a system with M ports all perfectly matched, we can pick port 1 as the input and consider the other ports as a form of dissipation. Due to the energy escaping from the other $(M - 1)$ ports, we will obtain a reflection coefficient S_{11} with magnitude less than one, which is similar to that obtained in the one-port lossy case (i.e., with losses due to finite wall conductivity). The cavity impedance seen from port 1, Z_1 , is calculated from S_{11} , one of the elements from the M by M scattering matrix,

$$Z_1 = R_R \frac{1 + S_{11}}{1 - S_{11}} + jX_R. \quad (31)$$

When normalized by the radiation impedance this corresponds to a complex impedance $\zeta_M = (1 + S_{11})/(1 - S_{11}) = \rho + j\xi$. On the other hand, we can generate the lossy one-port impedance ζ from Eq. (48) in Ref. [1], modelling the lossy effect by adding a small imaginary term to the frequency [5]. We can then compare the statistics of ζ from the lossy one port and ζ_M from the M -port lossless case (We note that approximate analytic formula for the distributions of the real and imaginary parts of ζ have recently been given by Fyodorov and Savin [21]). An appropriate value of the damping parameter in the one port case, $\tilde{k}^2\sigma$ ($\sigma = 1/Q$), can be determined so that the average value of $|S_{11}|^2$ in the lossy case is equal to $2/(M + 1)$ for the TRS case (or $1/M$ for the TRSB case). Then we can compare the real and imaginary parts of the impedances obtained in the two different ways. In Fig. 4, we include the results for the three different number of ports, $M=4, 13$ and 57 , and the corresponding one port result. For $M = 4$ we note that the distributions are similar but clearly not the same. However, for $M=13$ or 57 , the distributions for ζ and ζ_M are much closer. Thus, we confirm that distributed damping and a large number of output channels are equivalent so as to affect the distribution of the sub-unitary scattering matrix.

We now briefly discuss the multiport case with $M > 2$ and with mismatch ($|\rho_R| > 0$). As long as the assumption that the eigenfunctions (η) and the eigenvalues (θ or ϕ) are independent is still true, $\langle |S_{11}|^2 \rangle$ is related to the mismatch only through $\langle \cos(\phi_k - \phi_l) \rangle$, similar to the expression in Eq. (21). The same series of steps specified in the Appendix can be carried out to show that $\langle \cos(\phi_k - \phi_l) \rangle$, as well as $\langle |S_{11}|^2 \rangle$, depend only on $|\rho_R|$ (and are independent of the phase of ρ_R). We have verified this by numerical simulation using the impedance matrix generated from (11) with up to seven channels.

V. SUMMARY

We have generalized our random coupling model proposed in Ref. [1] to the multiport case. A similar impedance normalization is applied to obtain the statistical properties of the multiport chaotic scattering ma-

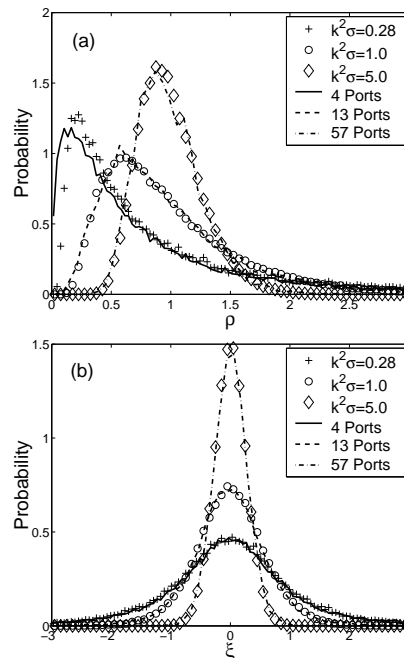


FIG. 4: Comparison between the impedance obtained from the one-port lossy case and the multiple lossless case. (a) for the real part of the impedance; (b) for the imaginary part of the impedance.

trix. The correlation coefficients between eigenvalues are calculated explicitly and agrees with the random matrix theory.

We further incorporate the coupling parameters γ_R and γ_X into the formulation of multiport scattering matrices and present the formula for the averaged reflection coefficients versus different values of coupling strength. We find that $|\rho_R|$, which is a function of the two parameters above, characterizes the transport process. For different pairs of (γ_R, γ_X) , as long as they yield the same value of $|\rho_R|$, the corresponding averaged reflection coefficients are the same. This observation may offer a useful criteria for cavity design.

Using HFSS, we test the conclusions above using impedance data calculated from direct numerical solution of Maxwell Equations. The agreement between the numerical results and the theoretical predictions convinces us that our approach of impedance normalization successfully recovers the statistical ensemble for chaotic scattering in the multiple port case.

Acknowledgments

We thank useful discussion with R. E. Prange, S. Fishman, J. Rogers and S. Anlage as well as comments from Y. Fyodorov and P. Brouwer. This work was supported in part by the DOD MURI for the study of microwave effects under AFOSR Grant F496200110374.

APPENDIX: EVALUATION OF $\langle |S_{11}|^2 \rangle$

In this appendix, we will start from the one-port case, and obtain an expression for the phase of S in term of the reflection coefficient ρ_R defined in Eq. (23). Then, using Eq. (13), we can evaluate $\langle \cos(\phi_1 - \phi_2) \rangle$ for the two-port in the TRS and TRSB cases.

In the one-port case, S can be expressed as

$$\begin{aligned} S = e^{j\phi} &= \frac{Z - Z_0}{Z + Z_0} \\ &= \frac{j(\gamma_X + \tilde{\xi}\gamma_R) - 1}{j(\gamma_X + \tilde{\xi}\gamma_R) + 1}, \end{aligned} \quad (\text{A.1})$$

where $\tilde{\xi}$ is a zero mean, unit width, Lorentzian random variable, which can be written as,

$$\tilde{\xi} = \tan \theta \quad (\text{A.2})$$

with θ uniformly distributed in $[-\pi/2, \pi/2]$. Putting Eq. (A.2) into Eq. (A.1), we get

$$e^{j\phi} = \frac{(\gamma_R + j\gamma_X - 1)e^{j\theta} - (\gamma_R - j\gamma_X + 1)e^{-j\theta}}{(\gamma_R + j\gamma_X + 1)e^{j\theta} - (\gamma_R - j\gamma_X - 1)e^{-j\theta}}. \quad (\text{A.3})$$

Introducing ρ_R such that

$$\gamma_R + j\gamma_X - 1 = \rho_R(\gamma_R + j\gamma_X + 1), \quad (\text{A.4})$$

and defining

$$e^{-j\alpha} = \frac{\gamma_R - j\gamma_X + 1}{\gamma_R + j\gamma_X + 1}, \quad (\text{A.5})$$

we obtain a compact expression for ϕ in term of θ and ρ_R ,

$$\begin{aligned} e^{j\phi} &= \frac{\rho_R - e^{-j(2\theta+\alpha)}}{1 - \rho_R^* e^{-j(2\theta+\alpha)}} \\ &= e^{j\phi_R} e^{-j2\theta'} \frac{1 + |\rho_R| e^{j2\theta'}}{1 + |\rho_R| e^{-j2\theta'}}, \end{aligned} \quad (\text{A.6})$$

where $2\theta' = (2\theta + \alpha + \pi + \phi_R)$. Since α and ϕ_R depend only on the coupling coefficient γ_R and γ_X , and 2θ is uniformly distributed in $[0, 2\pi]$, the angle $2\theta'$ is also uniform in $[0, 2\pi]$. Thus,

$$\begin{aligned} P_\phi(\phi) &= P_{2\theta'}(2\theta') \left| \frac{d(2\theta')}{d\phi} \right| \\ &= \frac{1}{2\pi} \frac{1}{1 + |\rho_R|^2 - 2|\rho_R| \cos(\phi - \phi_R)}. \end{aligned} \quad (\text{A.7})$$

The relation between ϕ and $2\theta'$ also holds true for multi-port cases. Furthermore, from the joint probability density function of $2\theta_1$ and $2\theta_2$ in Eq. (13), which is only a function of the difference of two angles, we find that $2\theta_1$ and $2\theta_2$ have the same joint distribution specified in Eq. (13). Thus we can evaluate

$$\begin{aligned} \langle \cos(\phi_1 - \phi_2) \rangle &= \text{Re}[e^{j\phi_1 - j\phi_2}] \\ &= \text{Re}\left[\frac{e^{-j2\theta'_1} + |\rho_R|}{1 + |\rho_R| e^{-j2\theta'_1}} \frac{e^{j2\theta'_2} + |\rho_R|}{1 + |\rho_R| e^{j2\theta'_2}} \right], \end{aligned} \quad (\text{A.8})$$

by using the joint distribution of $2\theta'_1$ and $2\theta'_2$, $P_\beta(2\theta_1, 2\theta_2) \propto |e^{j2\theta'_1} - e^{j2\theta'_2}|^\beta$, where $\beta = 1$ corresponds to the TRS case, and $\beta = 2$ for TRSB case.

Introducing $\psi_1 = 2\theta'_1$, $\psi_2 = 2\theta'_2$, and their difference $\psi_- = \psi_1 - \psi_2$, we obtain for the average of $\cos(\phi_1 - \phi_2)$,

$$\begin{aligned} \langle \cos(\phi_1 - \phi_2) \rangle &= \iint \frac{d\psi_1 d\psi_2}{(2\pi)^2} P(\psi_1, \psi_2) \\ &\quad \text{Re}\left[\frac{e^{-j\psi_1} + |\rho_R|}{1 + |\rho_R| e^{-j\psi_1}} \frac{e^{j\psi_2} + |\rho_R|}{1 + |\rho_R| e^{j\psi_2}} \right] \\ &= \int \frac{d\psi_-}{2\pi} P(\psi_-) \\ &\quad \text{Re}\left[\int_0^{2\pi} \frac{\psi_2}{2\pi} \frac{e^{-j(\psi_- + \psi_2)} + |\rho_R|}{1 + |\rho_R| e^{-j(\psi_- + \psi_2)}} \right. \\ &\quad \left. \frac{e^{j\psi_2} + |\rho_R|}{1 + |\rho_R| e^{j\psi_2}} \right]. \end{aligned} \quad (\text{A.9})$$

The inner integral can be calculated by introducing a complex variable $z = e^{j\psi_2}$ in terms of which the inner integral becomes

$$\frac{1}{2\pi j} \oint_{\text{unit circle}} \frac{dz f(z)}{z(z + |\rho_R| e^{-j\psi_-})}, \quad (\text{A.10})$$

where $f(z) = (|\rho_R|z + e^{-j\psi_-})(z + |\rho_R|)/(1 + z|\rho_R|)$. Evaluating this integral via the residues at the two poles within the unit circle, $z = 0$ and $z = -|\rho_R| e^{-j\psi_-}$, we obtain

$$\begin{aligned} \langle \cos(\phi_1 - \phi_2) \rangle &= \int_0^{2\pi} \frac{d\psi_-}{2\pi} P(\psi_-) \\ &\quad \left[1 - \frac{(1 - |\rho_R|^4)(1 - \cos \psi_-)}{1 + |\rho_R|^4 - 2|\rho_R|^2 \cos \psi_-} \right]. \end{aligned} \quad (\text{A.11})$$

For the TRS case, $P_{\psi_-}(\psi_-) = \pi |\sin(\psi_-/2)|/2$, and Eq. (A.11) yields

$$\begin{aligned} \langle \cos(\phi_1 - \phi_2) \rangle &= \frac{|\rho_R|^4 + 2|\rho_R|^2 - 1}{2|\rho_R|^2} \\ &\quad + \frac{(1 - |\rho_R|^2)^3}{4|\rho_R|^3} \ln \frac{1 + |\rho_R|}{1 - |\rho_R|}. \end{aligned} \quad (\text{A.12})$$

For the TRSB case, $P_{\psi_-}(\psi_-) = 2 \sin^2(\psi_-/2) = (1 - \cos \psi_-)$, and (A.11) yields

$$\langle \cos(\phi_1 - \phi_2) \rangle = 1 - \frac{(|\rho_R|^2 - 1)(|\rho_R|^2 - 3)}{2}. \quad (\text{A.13})$$

-
- [1] X. Zheng, T. M. Antonsen and E. Ott *accepted by Electromagnetics*, (2004), preprint cond-mat/0408327.
- [2] T. J. Krieger, *Ann. of Phys.* **42**, 375(1967).
- [3] Y. Alhassid, *Rev. Mod. Phys.* **72**, 895 (2000); C. W. J. Beenakker, *Rev. Mod. Phys.* **69**, 731 (1997).
- [4] P. A. Mello, *J. Phys A* **23**, 4061(1990).
- [5] E. Doron, U. Smilansky and A. Frenkel, *Phys. Rev. Lett.* **65**, 3072(1990).
- [6] S-H. Chung, A. Gokirmak, D. Wu, J. S. A. Bridgewater, E. Ott, T. M. Antonsen and S. M. Anlage, *Phys. Rev. Lett.* **85**, 2482(2000).
- [7] R. A. Méndez-Sánchez, U. Kuhl, M. Barth, C. H. Lewenkopf and H. -J Stöckmann, *Phys. Rev. Lett.* **91**, 174102 (2003).
- [8] S. Hemmady, X. Zheng, E. Ott, T. M. Antonsen and S. M. Anlage, *accepted by Phys. Rev. Lett.*(2004), cond-mat/0403225.
- [9] J. Barthélemy, O. Legrand, and F. Mortessagne, preprint (2004), cond-mat/0401638, submitted to *Phys. Rev. E*; J. Barthélemy, O. Legrand, and F. Mortessagne, preprint (2004), cond-mat/0402029, submitted to *Phys. Rev. Lett.*
- [10] P. Seba, Karl Zyczkowski, and J. Zakrzewski, *Phys. Rev. E*, **54**, 2438 (1996)
- [11] Y. V. Fyodorov and H. J. Sommers, *J. Math. Phys.* **38**, 1918 (1997).
- [12] M. L. Mehta, *Random Matrices*, second edition (Academic Press, 1991); K. B. Efetov, *Adv. Phys.* **32**, 53 (1983).
- [13] L. K. Warne, K. S. H. Lee, H. G. Hudson, W. A. Johnson, R. E. Jorgenson and S. L. Stronach, *IEEE Trans. on Anten. and Prop.* **51** 978 (2003).
- [14] P. A. Mello, P. Peveyra, and T. H. Seligman, *Ann. of Phys.* **161**, 254 (1985).
- [15] U. Kuhl, M. Martínez-Mares, R. A. Méndez-Sánchez and H. -J. Stöckmann, preprint (2004) cond-mat/0407197.
- [16] M. V. Berry *J. Phys. A.* **10** 2083 (1977); Y. Alhassid, and C. H. Lewenkopf, *Phys. Rev. Lett.* **75** 3922 (1995).
- [17] E. Kogan, P. A. Mello, and H. Liqun, *Phys. Rev. E*, **61**, R17 (2000).
- [18] J. F. Cornwell, *Group Theory in Physics: an Introduction* (Academic Press, San Diego, California, 1997).
- [19] P. A. Lee and T. V. Ramakrishnan, *Rev. Mod. Phys.* **57**, 287 (1985); G. Bergmann, *Phys. Rep.* **107**, 1 (1984).
- [20] P. W. Brouwer and C. W. J. Beenakker, *Phys. Rev. B* **55** 4695 (1997); R. Schäfer, T. Gorin, T. H. Seligman and H. -J Stöckmann, *J. Phys. A* **36** 3289 (2003).
- [21] Y. V. Fyodorov and D. V. Savin, preprint (2004) cond-mat/0409084; D. V. Savin and H. -J. Sommers, *Phys. Rev. E* **69** 035201 (2004); D. V. Savin and H. -J. Sommers, *Phys. Rev. E* **68**, 036211 (2003).